

We are IntechOpen, the world's leading publisher of Open Access books Built by scientists, for scientists

4,800

Open access books available

122,000

International authors and editors

135M

Downloads

Our authors are among the

154

Countries delivered to

TOP 1%

most cited scientists

12.2%

Contributors from top 500 universities



WEB OF SCIENCE™

Selection of our books indexed in the Book Citation Index
in Web of Science™ Core Collection (BKCI)

Interested in publishing with us?
Contact book.department@intechopen.com

Numbers displayed above are based on latest data collected.
For more information visit www.intechopen.com



Polarization Remote Sensing for Land Observation

Lei Yan, Taixia Wu and Xueqi Wang

Additional information is available at the end of the chapter

<http://dx.doi.org/10.5772/intechopen.79937>

Abstract

In the real world, vegetation, liquid surfaces, rocks, buildings, snows, clouds, fogs, etc. can all be regarded as natural polarizers. In the process of reflecting, transmitting, and scattering of electromagnetic radiations, land surface objects can produce polarized features that are related to the nature of the materials. These polarized information can determine objects' properties, and therefore, detecting the polarization information of objects becomes a new method of remote sensing. Polarization of reflected and scattered solar electromagnetic radiation adds a new dimension to the understanding of the Earth's objects' properties. The polarized bidirectional reflectance characteristics and polarized hyperspectral properties of land objects were methodically studied. The results of the polarized bidirectional reflectance characteristics can provide the theoretical basis for polarization remote sensing such as the detecting conditions, modeling and others. The polarized spectral property of the typical objects can be used as the spectral basis for polarization remote sensing. The atmospheric correction is a key problem when using polarization remote sensing method to detect land objects' information, because scattered atmospheric particles exhibit stronger polarization phenomena than land objects do. A method of using atmospheric neutral point for the separation polarization effect between objects and atmosphere has been proposed.

Keywords: polarized light, remote sensing, Earth's observation

1. Introduction

Besides properties such as intensity, frequency, and coherence, polarization is another fundamental character of electromagnetic radiation. The polarization phenomenon occurs along with the entire process of electromagnetic radiation reflection, scattering, and transmission. Since the discovery of the scattered light from the blue sky is polarized by D.F.J. Arago in 1809, the effects of various polarization parameters have been observed and measured by many scientists [1].

All of these results have clearly indicated that aerosols and natural land surfaces have large polarization effects, which, therefore, offers a powerful tool for monitoring the aerosol and land objects' properties from space. While the intensity information tells us about materials, polarization presents information about surface features, shape, shading, and roughness. Polarization information has the potential to enhance many fields of optical metrology. Just like the space applications of the polarization of microwave radiation, space polarization measurement programs are needed in the visible and near-IR spectral regions for better monitoring of the Earth's environment. Polarization of reflected and scattered solar radiation adds a new dimension to the understanding of the Earth's environmental radiation field. Furthermore, with the quick development of remote sensing, the numerical solution of the remote sensing retrieval process leads to the so-called, ill-posed inverse problem [2]. This problem is characterized by the incompleteness of the available information, the nonuniqueness of the solutions, and the noncontinuous dependence of the solutions on the input data. The polarization measurement not only can provide the intensity information of land surface objects, but also can provide some extra parameters, such as degree of polarization, polarization angle, and polarization phase information, all beneficial for the solution of the ill-posed inverse problem [3].

Currently, the research of polarization remote sensing focuses mainly on the atmosphere and climate [4, 5]. It is mainly because polarization complements the spectral and angular radiance measurements, and it produces a high sensitivity to microphysical properties of aerosol particles than do radiance measurements. Furthermore, the satellite polarization sensor POLDER's 6-km pixel size spatial resolution is a benefit for broad-scale (such as atmosphere) researches [6]. However, some researchers have found that objects on the land objects surface have strong polarized reflection. Tamalge and Curran gave a review of early attempts to use polarization information for land surface remote sensing [7]. Theoretical studies also were performed to understand the nature of polarization and to model the polarization from earth surfaces [8]. Until now, most studies were focused on atmospheric polarization than land surfaces because the polarization effect of the atmosphere is much stronger than that of land objects. Removing the atmospheric effect, therefore, would solve the bottleneck problem of using polarized information for remote sensing land surface. As a result, a major concern for the use of polarized light for the study of land surfaces is the capability to discriminate between polarization generated in the atmosphere and that generated by the surface.

2. Polarization characters of land objects

Polarization is defined as the asymmetry of vibration direction relative to spreading direction. It is a unique feature of horizontal wave. Polarization is an important feature of electromagnetic wave. Objects on the land and in the atmosphere can produce their unique polarized signals during reflection, scattering, and transmission, which means, polarization can reveal abundant information of the objects. In the nature, natural polarizers exist here and there, such as smooth leaves of a plant, soil, water surface, ice, snow, cloud, fog, etc. Reflection of sunshine by such polarizers can result in polarization. Based on this feature, polarized remote sensing

provides new and potential information for objects. And polarized remote sensing has become a new Earth observation method, which is receiving more and more attention [9].

According to electromagnetic theory, light is a horizontal wave and it vibrates vertically to the transmissive direction. Based on the trajectory of light vibration, it has five polarization states: natural light (nonpolarized light), linearly polarized light, partially polarized light, round polarized light, and elliptically polarized light. Natural light has same vibration range in every direction. It may vibrate in each direction that is vertical to its spreading direction with same amplitude. If we decompose the light of all directions to only two vertical directions, then we can find the same vibration energy and amplitude in the two directions. Linear polarized light means that in the vertical plane to the spreading direction, light vector only vibrates toward a certain direction. Partial polarized light can be viewed as a mix of natural light and linearly polarized light; namely it has a vibration range in a certain direction that is superior to other directions. Round polarized light and elliptical polarized light refer to light whose vector end has a round or elliptical trajectory on the vertical plane.

Polarized light is normally embodied as elliptical polarization. We need three mutually independent parameters to describe elliptical polarization light, for example, amplitude E_x, E_y and phase difference δ (or elliptical length, short axis a, b and angle of orientation ψ). Stokes raised "Stokes Parameter" in 1852. And it became the three mostly used macromasurable parameters. Stokes parameters not only can describe complete polarized light, but also partially polarized light.

Stokes Vector has four parameters (three of them are mutually independent). They can be shown as follows, and this set of parameters is called Stokes Vector.

$$S = [S_0 \ S_1 \ S_2 \ S_3]^T \quad (1)$$

The four Stokes parameters, which can be marked as S_0, S_1, S_2, S_3 , are defined as:

$$\begin{aligned} S_0 &= \langle \tilde{E}_x^2(t) + \tilde{E}_y^2(t) \rangle \\ S_1 &= \langle \tilde{E}_x^2(t) - \tilde{E}_y^2(t) \rangle \\ S_2 &= 2\langle \tilde{E}_x(t) \cdot \tilde{E}_y(t) \cos \delta \rangle \\ S_3 &= 2\langle \tilde{E}_x(t) \cdot \tilde{E}_y(t) \sin \delta \rangle \end{aligned} \quad (2)$$

\tilde{E}_x, \tilde{E}_y are components of electric vector along x, y in the selected coordinate, δ is the phase difference between two vibration components, and $\langle \rangle$ means taking the average of time. This four-dimensional vector can embody the status of any polarized light including polarization degree. S_0 in the above equation represents polarization light intensity, S_1 represents linear polarization light component, S_2 for in 45° linear polarization light component direction, and S_3 for dextrorotation circular polarization light component.

Based on Stokes Vector, we can get polarization status information of any light as below:

$$\psi = \frac{1}{2} \arctan \frac{S_1}{S_2} \quad (3)$$

$$P = \sqrt{S_1^2 + S_2^2 + S_3^2} / S_0 \quad (4)$$

Herein, ψ is the azimuth angle of ellipse, which is also its orientation. P is a description of polarization degree of partially polarized light, and its value ranges from 0 under nonpolarized light to 1 under complete polarization. For partially polarized light, P will be the mid-value. Sometimes, I , Q , U , V are also used to replace S_0 , S_1 , S_2 , and S_3 [10, 11].

2.1. Objects surfaces show polarized characteristic mechanism

When light is slantwise, it irradiates the land objects' surface, parts of the irradiation is reflected, and the rest is absorbed by the objects. Assuming the incidence angle is α , the refraction angle is β , and the incidence light, the reflection light and the refraction light compose in the main plane. Regardless of which vibratory direction of the incidence light is, its electric vector can be decomposed to two components: the vertical component $E_{10\perp}$ and the parallel component $E_{10=}$. Also supposing the corresponding electric vector components of the reflection light are $E'_{10\perp}$ and $E'_{10=}$, the corresponding electric vector components of the refraction light are $E_{20\perp}$ and $E_{20=}$.

When nonpolarized light reflected and refracted by the two media interfaces, the radiate directions of the reflection and refraction lights are determined by the law of reflection and refraction; however, the vibratory directions of these two lights, namely the polarization state, obey the electromagnetic theory of light. Based on the Fresnel formula, the electric vector's reflection radiant intensity of the vertical and the parallel component is as follows:

$$E'_{10\perp} = -\frac{\sin(\alpha - \beta)}{\sin(\alpha + \beta)} \cdot E_{10\perp} \quad (5)$$

$$E'_{10=} = \frac{\tan(\alpha - \beta)}{\tan(\alpha + \beta)} \cdot E_{10=} \quad (6)$$

$$\frac{E'_{10=}}{E_{10=}} = \frac{E'_{10\perp}}{E_{10\perp}} \cdot \frac{\cos(\alpha + \beta)}{\cos(\alpha - \beta)} \quad (7)$$

When $\alpha = 0^\circ$, because of $E_{10\perp} = E_{10=}$, so

$$E'_{10=} = E'_{10\perp} \quad (8)$$

These two components are irrelevant. After being synthesized, the reflection light is still unpolarized. Thereby, the polarization does not exist in the reflection light when the incidence light irradiates objects vertically.

When $0^\circ < \alpha < 90^\circ$,

$$|\cos(\alpha + \beta)| < \cos(\alpha - \beta) \quad (9)$$

Then, we get

$$\frac{E'_{10=}}{E_{10=}} < \frac{E'_{10\perp}}{E_{10\perp}} \quad (10)$$

From formulae (5) and (6), we found that the physical effects of the two components $E_{10\perp}$ and $E_{10=}$ are different. No matter what the polarization state of the incidence light is, the interface reflects $E_{10\perp}$ as shown in formula (5) and reflects $E_{10=}$ as shown in formula (6). Formula (10) indicates that in the reflection light, the parallel component $E'_{10=}$ is always smaller than the vertical component $E'_{10\perp}$. These two components are vector sum in the two directions that include massive polarized light of different amplitudes and different directions. Therefore, these two components are irrelevant and cannot synthesize a vector. So, the polarization state is different from the incidence light [9].

2.2. The polarized directional characteristic of land objects

The bidirectional reflectance is the common macrophenomenon of the electromagnetic wave reflection in nature. It reveals that the reflection has directivity relying on the incident direction. The ability of reflecting and dispersing the electromagnetic wave of targets are closely related to its surface structural characteristic and material composition, the surface of various targets could radiate the incident electromagnetic wave in any directions (except absorption) and form different fringing flux function of material spectrum characteristic. It has been expounded by bidirectional reflection distribution function (BRDF). In the following discussion, the observation that does not add polarized radiance is bidirectional reflection.

The multiangle polarization remote sensing intends to utilize the polarization characteristic information of the targets on ground or in air. During the process of reflecting, scattering, and transmitting the electromagnetic radiation, the multiangle polarization remote sensing can produce polarized bidirectional reflection as the remote sensing information source.

During reflection, scattering, and transmission, multiangle spectral feature and polarized feature based on intrinsic characteristics of land objects exist. By studying the multiangle spectral feature and polarized feature, their directional reflectance laws and polarized reflectance laws in 2π space can be identified. Those potential laws, together with abundant information about angle and polarization, bring new methods for remote sensing application [12].

We measured multiangle polarization reflectance and bidirectional reflectance of different types of soils, including brown forest soil, calcareous soil, clay soil, yellow soil, and humus soil with different water content using bidirectional photometer device. The light source angles and viewing zenith angles range from 0 to 60° with 10° interval, the relative azimuth between the source and the sensors (180° is the specular direction) from 0 to 360° with 10° interval. Polarizer was attached in front of the light source and can be rotated freely. The maximum polarized reflectance data were measured when the pointer was at 90° , while the minimum

polarized reflectance data were measured when the azimuth was at 0° . Once the polarized data are collected, a white panel reflectance was measured immediately. Then, the ratios of the polarization and the reference data were calculated automatically. The results were stored in a database. Brown forest soil (collected from Liaoning province, China, water content is 19.7%) was taken as an example.

2.2.1. The influence of the incidence angle

Figures 1–3 show the 0 and 90° polarized reflectance spectra of brown forest soil at 670–690 nm spectral bands, and the incidence angles are 20 , 40 , and 60° respectively. In the figure, the abscissa denotes the relative azimuth angle (θ) from 90 to 270° and different designs denote different viewing zenith angles (φ) from 0 to 60° . All the data cover the 2π space of brown forest soil's surface.

In **Figure 1**, the curve of 20° incidence angle shows no obvious wave crest in the specular direction. In **Figures 2** and **3**, the curves with viewing zenith angles of 40 , 50 , and 60° show obvious wave peaks in the specular direction. The results indicate that with the increase of incidence angle from 10 to 60° , the spectral curves of brown forest soil in 2π space are changing gradually.

These results suggest that when the incidence angle is small, the reflection spectra of soil surface are characterized by diffuse reflection. There is almost no composite of specular and diffuse reflections. When the incidence angle increases, the reflection spectra show a specular reflection pattern. So, it is reasonable to think that there is a composite of specular and diffuse reflections. The incidence angle has influence on whether there will be a composite of specular and diffuse reflection.

2.2.2. The influence of viewing zenith and relative azimuth angle

Figure 1 shows when the incidence angle is small, the reflection spectra of the brown forest soil surface in 2π space have no obvious difference. The surface, thus, can be considered as a Lambert object. In **Figures 2** and **3**, when the viewing zenith angle is 40 – 60° , the spectral curves lost the Lambert characteristics. Because of the specular effect, there appears a wave crest in the azimuth

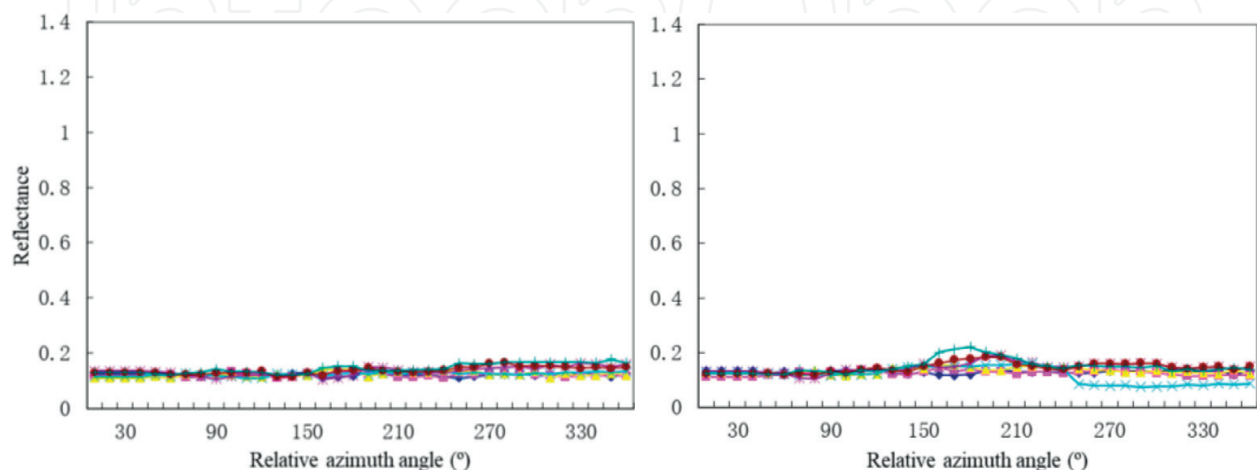


Figure 1. Polarized reflectance (0 and 90°) of brown forest soil at 670–690 nm, incidence angle = 20° .

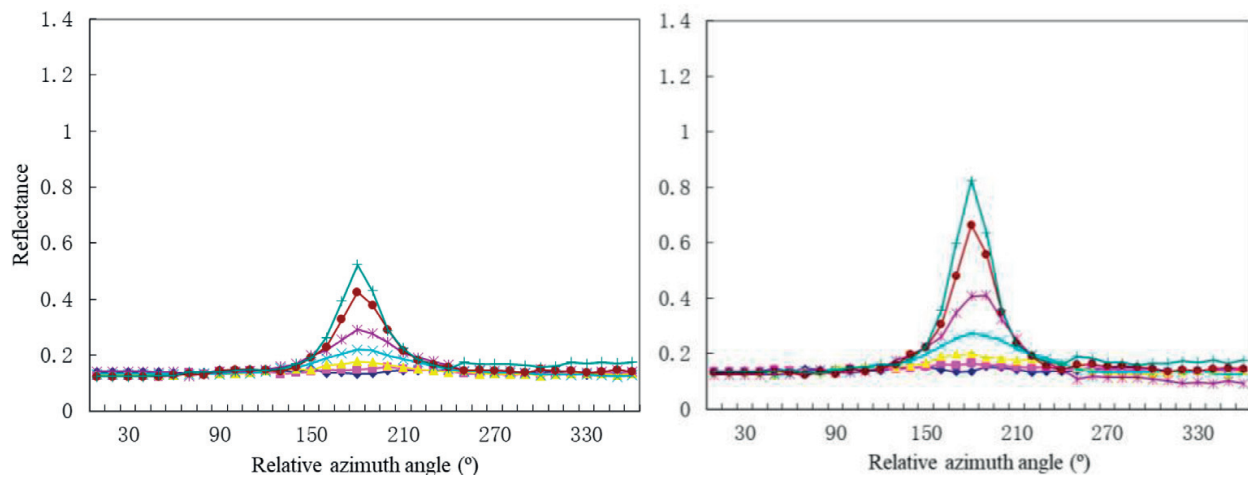


Figure 2. Polarized reflectance (0 and 90°) of brown forest soil at 670–690 nm, incidence angle = 40°.

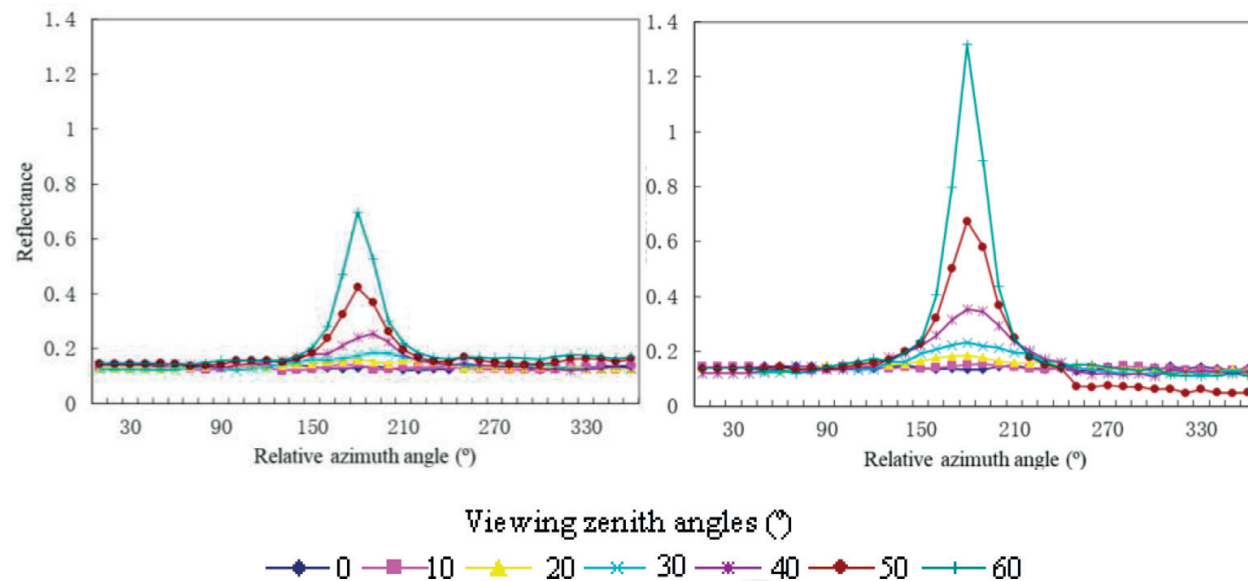


Figure 3. Polarized reflectance (0 and 90°) of brown forest soil at 670–690 nm, incidence angle = 60°.

of 135–225°. The height of the wave crest changes according to the size of viewing zenith angle. The curve for 30° has a relatively low crest, while those for 40, 50, and 60° are higher. The 180° azimuth angle is the specular direction. This phenomenon indicates that the specular effect of soil’s surface is intensified when the viewing zenith angle increases, thus losing ordinary Lambert characteristics.

2.3. Polarized spectral of land objects

Polarized hyperspectral imaging is a new remote sensing method combining the benefits of polarized and hyperspectral information [13]. It has hundreds of polarized wavelengths per spatial pixel. Polarized hyperspectral imaging combines traditional two-dimensional remote sensing imaging technology and polarized spectroscopy [14, 15], allowing to obtain both

images and polarized spectra of objects. The polarization measurement can not only get the intensity information of land surface objects, but can also get extra parameters, such as the degree of polarization (DoP), angel of polarization (AoP), and polarization phase information. This gives people the capability to discriminate, classify, and identify materials present in the image. Using a self-developed polarized field imaging spectrometer system (FISS-P), we collected the polarized hyperspectral images for several vegetations [16].

Ten related polarization parameters were considered in this study: I , Q , U , $DoLP$, AoP , R_0 , R_{60} , R_{120} , R , R_l . Here, I , Q , and U are the three Stokes parameters; $DoLP$ and AoP are the degree of linear polarization and angle of polarization, respectively; 0 , 60 , and 120° are the reflectances of three polarization azimuth angles, respectively; R is the nonpolarized reflectance; and R_l is the reflectance of I .

Figure 4 shows the $DoLP$, AoP , and reflectance contrast spectral curves of a *S. spectabile* leaf of the same pixel. The reflectance spectral curve of the leaf shows a typical vegetation reflectance spectral curve shape. The reflectance is low in both blue (450 nm) and red (690 nm) regions of the spectrum due to the absorption by chlorophyll in photosynthesis. It has a peak in green (540 nm) region. In near-infrared (700–800 nm) region, the reflectance is much higher than that in visible band due to the cellular structure in the leaves.

The AoP spectral curves of the leaf for the entire spectrum almost run parallel to the x-axis, and its values are all approximately equal to 0.5, indicating that the AoP spectral curves of the *S. spectabile* leaf have no unique spectral characteristics. It is not possible to use the AoP spectral curve as a recognition characteristic for *S. spectabile* leaves.

As for the $DoLP$ spectral curves of the leaf, the reflectance is high in both blue (450 nm) and red (690 nm) regions of the spectrum. It exhibits a wave valley in green (540 nm) region. In near-infrared (700–800 nm) region, the reflectance is much lower than in visible band. The data show visible and near-infrared bands, and the $DoLP$ and reflectance spectral curves of *S. spectabile* show contrasting trends.

Figure 5 displays the false color composite images of different parameters. The RGB bands of the three composite bands are the 167th band (666.8 nm), 243th band (771.3 nm), and 340th band (906.7 nm) of the FISS image. **Figure 5(a)** is the spectrum image cube of R ; **Figure 5(b–d)** is the I , Q , U images, respectively; and **Figure 5(e)** and **(f)** is the $DoLP$ and AoP images, respectively. The white area of **Figure 5(a)** and **(b)** is the white plate.

2.4. The polarization remote sensing method for water surface sun flare elimination

The sun flare produced by water mirror reflection is one of the main noises of the water color satellite images. It is an important subject to research on the sun flare and the sun flare eliminating method in remote sensing. In order to avoid the sun flare, people often set the satellite Central European Time (CET) to 12 o'clock at noon or design the sensor into multiangle scan states. However, those two methods are unable to avoid the sun flare effectively because most satellite can only broadcast vertical observation. Here, a new method for this question is presented. Combining multiangle remote sensing with polarized light, the multiangle polarized reflection method about eliminating the sun flare and the suitable time of the polarized remote sensing of

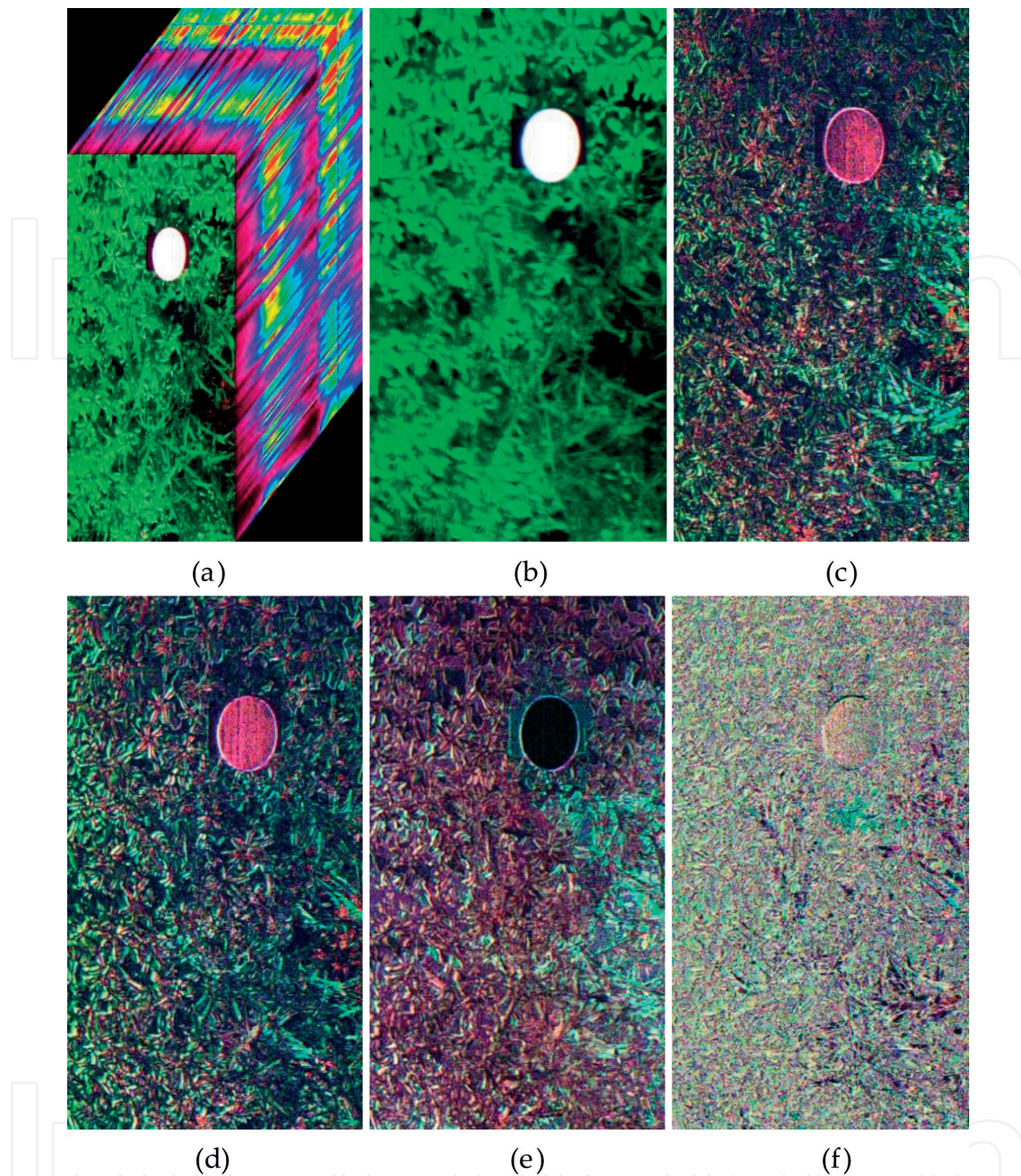


Figure 4. The *DoLP*, *AoP*, and reflectance spectral curves of a *Sedum spectabile* leaf. (a) Spectrum image cube of R, (b) I image, (c) Q image, (d) U image, (e) DoLP image, and (f) AoP image.

the water are proposed. This method will improve the utilization of the water color remote sensing images and the precision of the quantitative remote sensing.

2.4.1. Function of solar zenith and degree of polarization

When satellite CET moves from forenoon to 12 o'clock at noon, the central position of the solar flare moves from the image's east margin to the image's center; with the covering range of the solar flare changing from big to small, the distributing shape changing from long melon seeds shape to the ellipse with area gradually decreases, to a small flare at 12 o'clock at noon. When

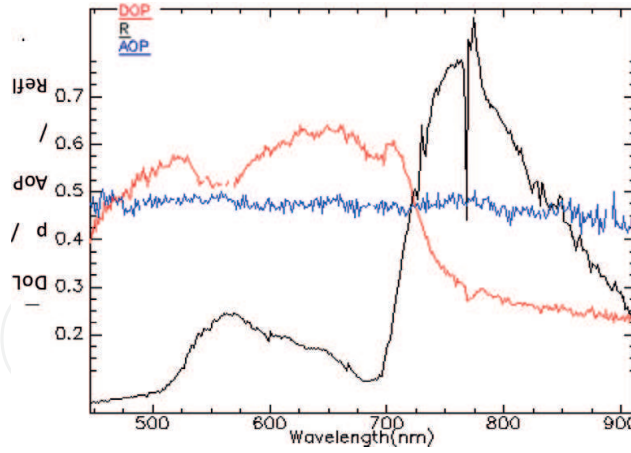


Figure 5. False-color composite images of different parameters (hyperspectral image (a), calculated Stokes parameters (*I*, *Q*, *U*) image (b, c, d), degree of linear polarization (DoLP) image (e), and angle of polarization image (f)).

the satellite CET’s moving continues, the situation is just on the opposite—the solar flare’s center moves toward the image’s west margin, and the influence to the image by the sun gradually becomes greater. The movement of the satellite to the solar is the relative movement; so the solar’s altitude angle is one of the main factors influencing the water surface solar flare’s formation, size, and distributing shape.

The polarization degree is the physical quantity describing the polarized light’s polarization degree, which expresses the proportion of the whole light taken by the linearly polarized light quantificationally. According to Fresnel formula, and because the light intensity is the square of the electric vector’s amplitude, then

$$P = \frac{E_{10\perp}^2 \frac{\sin^2(\alpha-\beta)}{\sin^2(\alpha+\beta)} - E_{10\parallel}^2 \frac{\cos^2(\alpha-\beta)}{\cos^2(\alpha+\beta)}}{E_{10\perp}^2 \frac{\sin^2(\alpha-\beta)}{\sin^2(\alpha+\beta)} + E_{10\parallel}^2 \frac{\cos^2(\alpha-\beta)}{\cos^2(\alpha+\beta)}} \quad (11)$$

where E_{\perp} is the component of the incident light whose electric vector is vertical to the incident interface, E_{\parallel} is the component of the incident light whose electric vector is parallel to the incident interface, α is the incidence angle, and β is the refraction angle.

When the incident light is the natural light, $E^2 = E_{\perp}^2 + E_{\parallel}^2$, using the refractive index to eliminate the refraction angle in Eq. (11), with the refractive index of the purified water is 1.33, yields

$$P = \frac{2 \sin \alpha \operatorname{tg} \alpha \sqrt{1.769 - \sin^2 \alpha}}{1.769 - \sin^2 \alpha + \sin^2 \alpha \operatorname{tg}^2 \alpha} \quad (12)$$

The derivative of the *P* function is then calculated when $P' = 0$, $\alpha = 53.1^\circ$. The maximum exists at this time in the function, that is, the reflected light is completely linearly polarized light, and the incidence angle α is the Brewster angle.

The reflected light’s DoP increases while the incidence angle α increases from 0° to Brewster angle gradually. When it gets to Brewster angle, the polarization degree is maximal, and then it

gradually decreases. That is to say, the closer to Brewster angle, the better the reflected light's linear polarization characteristics.

2.4.2. The mechanism of sun flare elimination

The water information received by the water color remote sensing sensors mainly contains three kinds of light: (1) the light that is directly reflected by the water surface, (2) the light that arrives at the sensors through the atmospheric photon scatters, and (3) the light that is backscattered from the water body. Only the third kind of light includes water body information, it is the only source of visible light remote sensing nearly, and the first two lights constitute the background noise that must be corrected and eliminated.

According to the above discussions, light after being reflected by the water body, the polarization phenomenon exists in the reflected light, and the water body is actually the polarizer at this time. When the light's incident angle is Brewster angle of 53° , that is, the sun's altitude angle is 37° , its reflected light is totally polarized light whose electric vector is vertical to the incidence interface. By using the polarizer in front of the sensor, the polarizer's azimuth angle is adjusted and the polarization angle is made just vertical to the polarization direction of the reflected light; at this time, the reflected light totally cannot pass through the polarization sheet due to the polarizer's light-blocking effect; the information received by sensors is the atmospheric scattering and volume scattering of water body, and the intensity of the water body mirror reflection can be ignored. So, we can use the radiation transfer equation (RTE) of the atmospheric and water to reckon the water quality indicators without the solar reflected light.

The angle between the horizon and the sun is sun's altitude angle, expressed in symbol h , which can be gained by the formula

$$\sin h = \sin \varphi \sin \delta + \cos \varphi \cos \delta \cos \tau \quad (13)$$

where φ stands for the local geographical latitude, δ is the solar declination angle, and τ is solar hour angle.

According to this formula, we can calculate the sun's altitude angle in any place on the earth at any time. Then, the suitable time for the water polarization remote sensing of all the world also can be figured out when the solar altitude angle equals to 37° . Here, we only list the timetable when the sun's altitude angle equals to 37° in the place around the world on vernal equinox day (**Table 1**). The suitable time is earlier or later than 12:00 at noon. On vernal equinox day $\delta = 0^\circ$, the time is the local time. Other time's dates can be deduced by analogy.

Table 1 shows that, on vernal equinox day, even at noon, the situation is impossible to exist that the sun's altitude angle equal to 37° in the areas exceeding south and north latitude is 53° ; we cannot use the polarization remote sensing to completely eliminate the water surface mirror reflection at this time.

Combining the local solar zenith angle, in the areas of south and north latitudes between 0 and 30° , there are 12 months in 1 year that the water surface mirror reflection can be completely avoided; in the areas of south and north between 30 and 40° , there are 8 months that the water surface mirror reflection can be completely avoided; the rest may be deduced

North latitude	0°	N10°	N20°	N30°	N40°	N50°	N53°	N60°
Suitable time (h)	12 ± 3:32:00	12 ± 3:29:19	12 ± 3:20:42	12 ± 3:03:55	12 ± 2:32:53	12 ± 1:22:16	12	—
South latitude	0°	S10°	S20°	S30°	S40°	S50°	S53°	S60°

The suitable time is the time when the solar altitude angle equals to 37°.

Table 1. The suitable time for water polarization remote sensing on vernal equinox day around the world.

by analogy, and in the polar region there is no time in the whole year that the water body surface mirror reflection can be completely avoided, because the sun's altitude angle is always lower than 37°.

The above discussion is the case of completely eliminating the sun flare, in fact, water glitter sometimes has useful information of water body. This information may play an important role for the water remote sensing retrieval. For example, the mirror reflection produced by the oil slick on water surface, and this information will be lost if we completely eliminate the glitter. In practice, the water body scattering is very weak, after completely eliminating the glitter, the water information received by the sensors will be too little to be detected because of the polarizer's absorption. On the other hand, it is hard to let the sensors' detection angle state at the Brewster angle. So, it is impossible and no need to completely eliminate the sun flare. As long as the sensor has not saturated by the glitter's radiation, the upward radiation of water will be identified effectively. That is to say, when the incident angle is nearby the Brewster angle, we can adjust the glitter's radiation by controlling the polarizer's azimuth. In this way, we can eliminate the noise and enhance the useful information.

Using different sensors, we can quantitatively present the suitable solar incident angle and the suitable polarization azimuth for the polarization remote sensing. It can keep the intensity of sun flare in an acceptable range and give the suitable schedule for the water polarization remote sensing. The suitable times will be much longer than the case that completely eliminates the sun flare. The sensor will receive more water information [17].

2.5. The polarized effect on plant spectrum

Leaf scattering spectrum is one of the key optical variables that conveys information about leaf absorbing constituents from remote sensing. It cannot be directly measured from space because the radiation scattered from leaves is affected by the three-dimensional canopy structure. In addition, some radiation is specularly reflected by the surface of leaves. This portion of reflected radiation is called partly polarized. It does not interact with pigments inside the leaf and therefore contains no information about its interior. Very few empirical data are available on the spectral and angular scattering properties of leaf surfaces. Whereas canopy structure effects are well understood, the impact of the leaf surface reflectance on estimation of leaf absorption spectra remains uncertain. We, thus, present empirical and theoretical analyses of spectral, angular, and polarimetric measurements of light reflected by needles and shoots of *Picea koraiensis* and *Pinus koraiensis* species. **Figure 6** illustrates our samples.

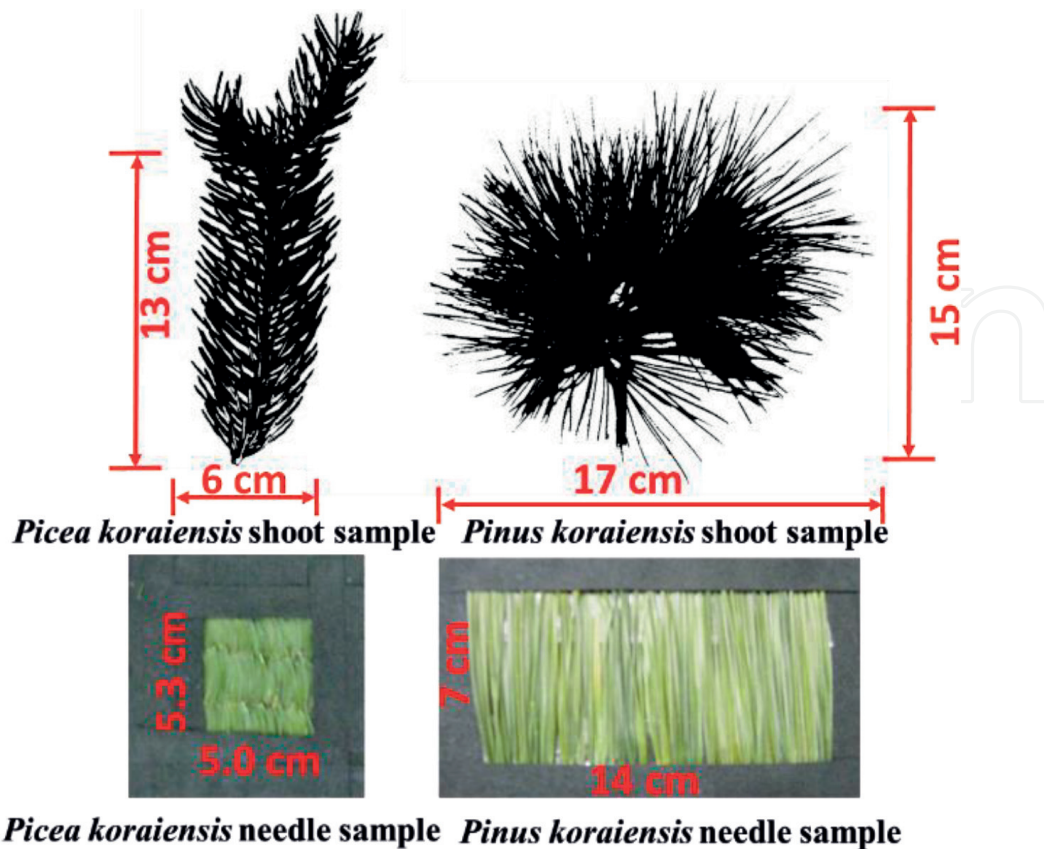


Figure 6. Samples of needles and shoots in the holder window. Sizes of the shoots were $13 \times 15 \times 17$ cm (*Pinus koraiensis*) and 6 cm (*Picea koraiensis*). Dimensions of the holder windows were $5.3 \times 7 \times 14$ cm (*Pinus koraiensis*) and 5.0 cm (*Picea koraiensis*).

The total radiation reflected by a leaf includes two components, diffuse and specular. The first component emitting from light reflected at the air-cuticle interface is polarized. The diffuse component results from photon interactions within the leaf and large particle on the leaf surface. This portion of reflected light is not polarized. Polarization measurements can help us to extract linearly polarization portion from the total radiation registered by the sensor. Radiation specularly reflected from the needle surfaces exhibits weak spectral dependency, as expected from theory. It increases from very small values in backscattering directions to about 17% in forward scattering directions. The shoot sample, polarized directional-conical reflectance factor (PDCRF), shows a similar phenomenon. Its magnitude, however, is reduced by a factor of about 10, as **Figure 7** shows.

Ignoring polarization portion in reflected radiation, however, can cause an overestimation of the scattering coefficient (**Figure 8**). The impact decreases from strongly (17–140%, 450–500 nm) to weakly (<4%, 800–950 nm) absorbing wavelengths.

To summarize, the spectral, angular, and polarimetric data convey information about properties of the needle surfaces, shoot structural organizations, and needle optics. This information is required to retrieve the needle albedo, which is directly related to the absorption spectra of leaf biochemical constituents [18].

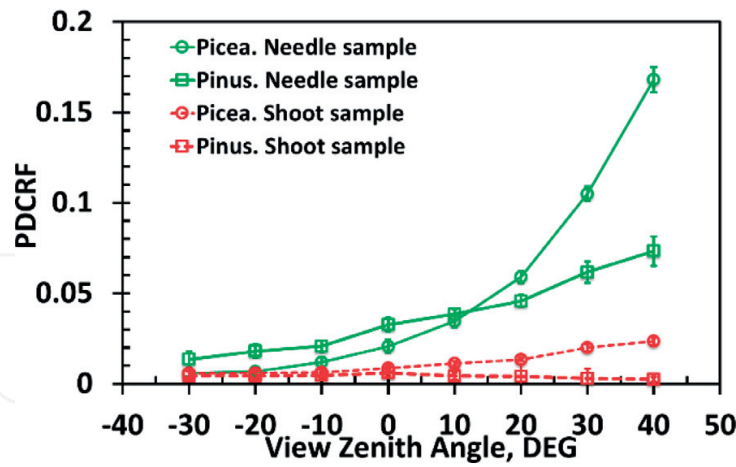


Figure 7. Angular distribution of average PDCRF of shoot samples (dashed lines) and needle samples (solid lines) averaged over 450–950 nm. Vertical bars denote ± 1 standard deviation.

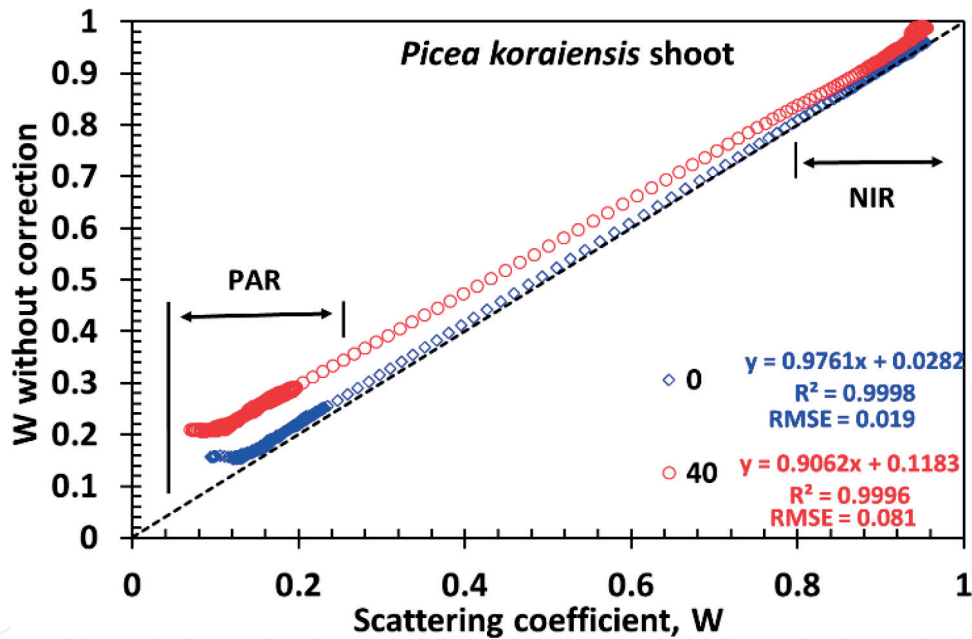


Figure 8. Correlation between scattering coefficients of the *Picea koraiensis* shoot derived with (horizontal axis) and without (vertical axis) correction for the needle surface effects. Relative differences are 17–140% in 450–500 nm, 3–74% in 600–650 nm, 3–59% in 520–580 nm, and below 4% in 800–950 nm spectral intervals.

3. Polarized remote sensing for atmospheric correction

Scattered atmospheric particles exhibit strong polarization phenomena. The polarization effect of the atmosphere is the main signal of the polarization remote sensing. For this reason, the present spaceborne polarization remote sensing data are mainly used for atmospheric research, such as to study the atmosphere physical properties and optical properties [19]. Land objects also have strong reflected polarization phenomenon and can be valuable information for remote sensing.

The land objects' detection was one of the tasks of the spaceborne polarimeter—POLarization and Directionality of the Earth's Reflectance (POLDER). However, studies found that the polarization effect of the atmosphere is much stronger than that of land objects in the images. Information on land object polarization received by the polarimeter is always submerged in the atmospheric polarization effect [20, 21]. As a result, a major concern for using polarized light for the study of land surfaces is the capability to discriminate between polarization generated in the atmosphere and that generated by the surface.

The neutral point is the point (or area) where the skylight is unpolarized. In the clear sky, there are three normally occurring neutral points, the Arago, Babinet, and Brewster neutral points, in the principal plane [22]. In this paper, we attempt to set spaceborne polarimeter to detect the Earth at the direction of the neutral point. Because the polarization effect of atmosphere is zero at this direction, the polarization information of the land surface objects can be maximized. This study would promote the polarized remote sensing for land objects detection and expand the polarization remote sensing research to a wider research area.

3.1. Atmospheric polarization distribution and neutral point

The solar radiation has no polarization at the outer space, and it will be polarized after the atmosphere particles is scattered. If most of the atmosphere scattering is single scattering, the polarization of the sky will show a regular polarization distribution, and it is also known as the polarization pattern of sky.

Under the clear sky weather conditions, in the vertical plane of sun, the Arago, Babinet, and Brewster neutral points in the sky will appear. As shown in **Figure 9**, the Arago is normally

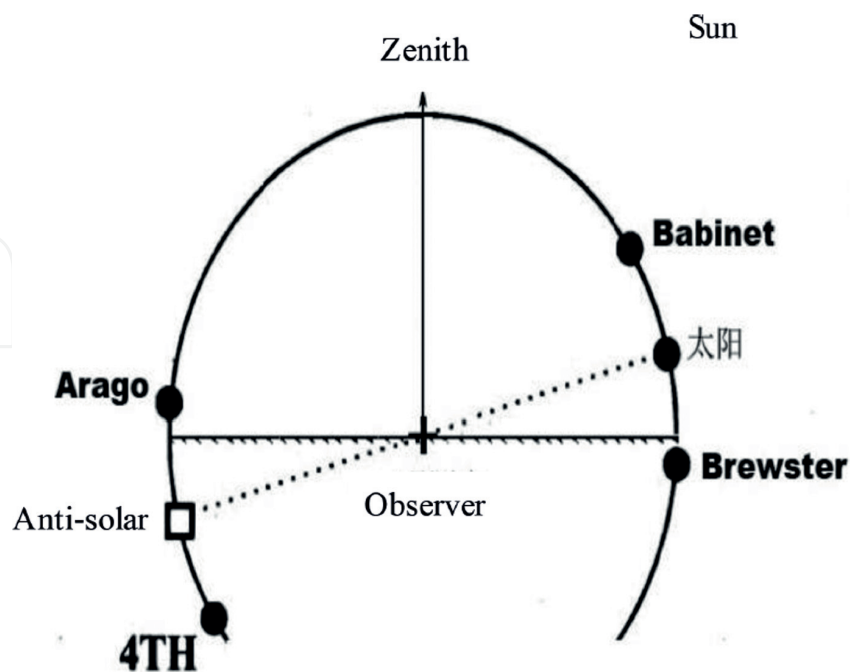


Figure 9. Relative positions of neutral points in the sky.

located $20\text{--}30^\circ$ above the antisolar point. The Babinet point is directly above the sun located at $15\text{--}20^\circ$. The Brewster point is directly below the sun varying from $15\text{--}20^\circ$. Both the Babinet and Brewster points are at the same direction of sun and their positions change along with the solar altitude. The higher the sun elevation angles, the closer between the Babinet point and the Brewster point. When the sun is at the zenith, the two points merged as one point [23, 24]. Because the neutral points at two side of sun and antisolar are symmetrical, there should be another neutral point under antisolar in theory, as the anti-Babinet neutral point. In 2002, the fourth neutral point actually has been detected using the sounding balloon [25].

For the single scattering, the polarization of the skylight is generally positive. However, for the multiple scattering, the atmospheric particles can cause negative polarization. The degree of polarization of sky will be zero where the positive and negative polarizations meet at the intersection area. In this way, the atmospheric neutral point is produced [26]. The neutral point is always at the main plane of the sun and zenith. The stronger the multiple scattering, there will be more negative polarization, and the neutral point position will be farther away from the theory position.

The positions of neutral points are close to the sun elevations. Chandrasekhar calculated positions of the three neutral points for various angles of incidence in the main plane. **Figure 10** shows the case for atmospheric optical thickness of 0.10. The abscissa and ordinate give the solar elevation angle and neutral point elevation angle, respectively.

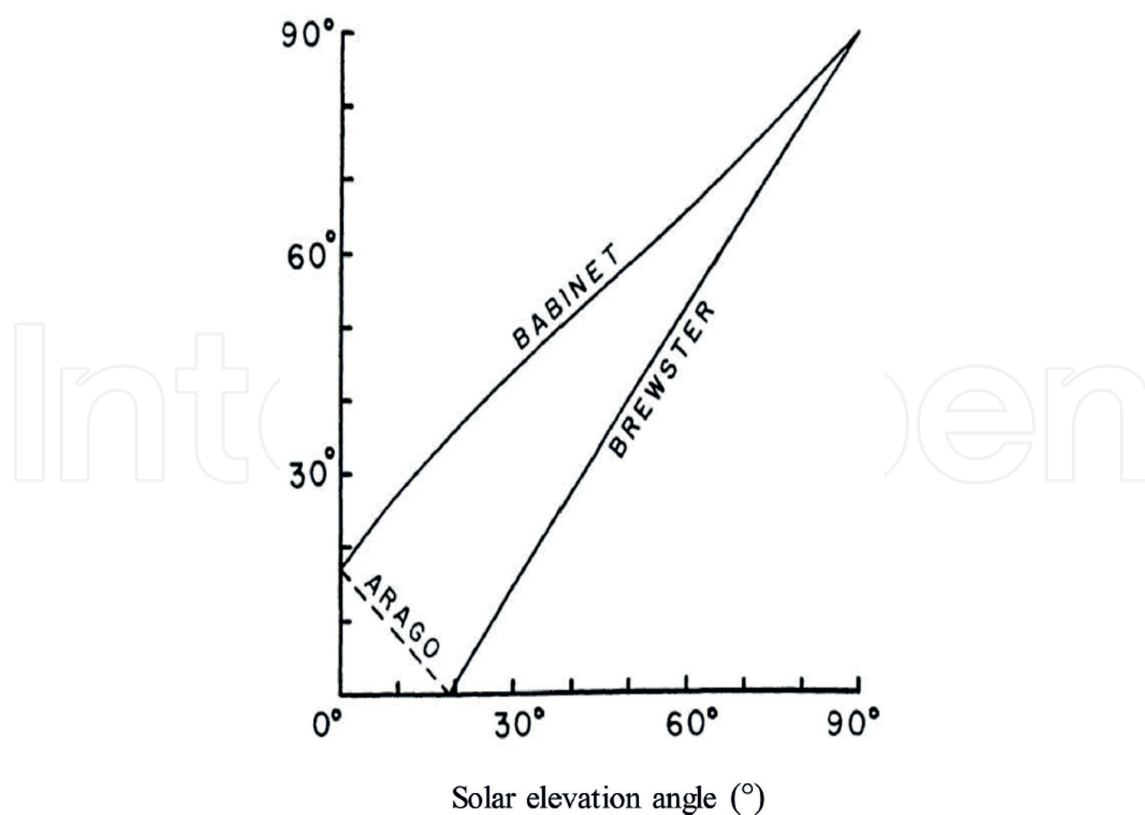


Figure 10. The relationship of neutral point and sun position.

Babinet point is visible throughout the day from before sunrise until after sunset. The Brewster neutral point becomes visible when solar elevation angle exceeds 20° . The position of the Brewster point and sun is almost linear. As for Arago point, it will appear when solar elevation angle is less than 20° . It means that the Arago point can only be observed in the morning or evening. The situation of other atmospheric optical thicknesses (0.15 or 0.20) is almost the same.

3.2. Atmosphere correction method based on neutral point

The method of using atmospheric neutral point for polarization remote sensing is to set the remote sensing sensor at the direction of the neutral point. At this moment, the atmospheric polarization effect between sensor and land objects can be zero or minimized. The polarization information of land objects received by sensor can be maximized. **Figure 11** is the sketch map of using neutral points for polarization remote sensing atmosphere correction. The dash circle is virtual outside the Earth's atmosphere. This circle is also the sun trail of the very day. The sun position in the figure is a virtual position too, which only denotes the direction of the sun in the figure. From space to land surface, the neutral point can be seen at each height in the line that goes through the neutral point and land object in theory. So, the neutral point can be observed through by airborne or spaceborne sensors.

In the real atmosphere, because of multiple scattering, the neutral point is probably not a point but a small region where all the degree of polarization is close to zero. In addition, this neutral point (region) in the sky is not a fixed position, but a conical region where starting point is the sensor as shown in **Figure 11**. The atmosphere degree of polarization at any height of this conical region is zero.

3.2.1. Neutral point characteristics observed from space

The positions of neutral points that we discussed above are based on ground observations; however, remote sensing is a process observed from sky to land. Can the remote sensing sensor

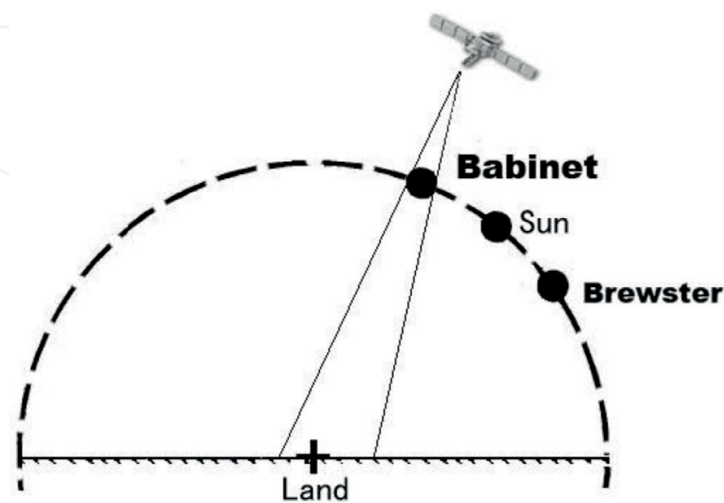


Figure 11. Sketch map of using neutral points for polarization remote sensing atmosphere correction.

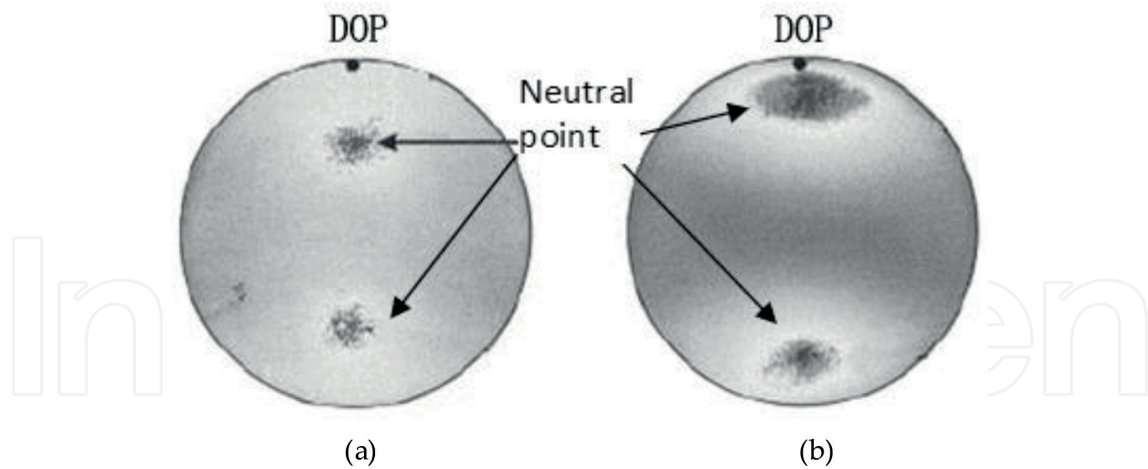


Figure 12. The neutral point observed from ground and space (the black areas are neutral points where DOP is nearly zero). (a) observed from ground, and (b) observed from space.

detect the neutral point from sky? It is the basic problem of using the neutral point for land surface polarization remote sensing.

Gábor Horváth [27] took the neutral point photos on the ground and at a 3500 m sounding balloon separately, as the dark areas shown in **Figure 12**. The local solar elevation angle shooting was similar to 0 when photos were taken. The black spot at the top of the image is the sun. The camera band was red. **Figure 12(a)** was the ground photo, while **Figure 12(b)** was the balloon photo. The right picture of **Figure 12(b)** indicates that the neutral point can be observed from space.

Coulson calculated the neutral point position of the atmosphere upward radiation and the downward radiation [28]. **Figure 13** shows the curve of angular distance between the sun and the neutral points as a function of sun elevation. The abscissa is the solar elevation angle and the ordinate is angular distance from neutral to antisolar. The atmosphere optical thickness is 1.0. The solid curves are the upward radiation and the dash curves are the downward radiation.

The upward radiation is caused by the backscattering of atmospheric particles. The neutral point's positions are different in the upward radiation and the downward radiation. So, the neutral points have different names in the upward radiation and the downward radiation. The neutral points observed from ground are Arago point, Babinet point, and Brewster point. And the corresponding neutral points observed from the space are Brewster point, anti-Babinet point, and Arago point.

In **Figure 13**, the solid and dash lines of curve (a) denote the neutral point below the antisolar and solar separately, which are Arago point and Brewster point. The solid and dash lines of curve (b) denote anti-Babinet point and Babinet point separately.

It can be seen from **Figure 13**, as for curve (a), that the neutral point positions in the upward and downward radiation are completely the same when the solar elevation angle is about 60° – 90° . Their positions began to differ greatly when the solar elevation angle changed from

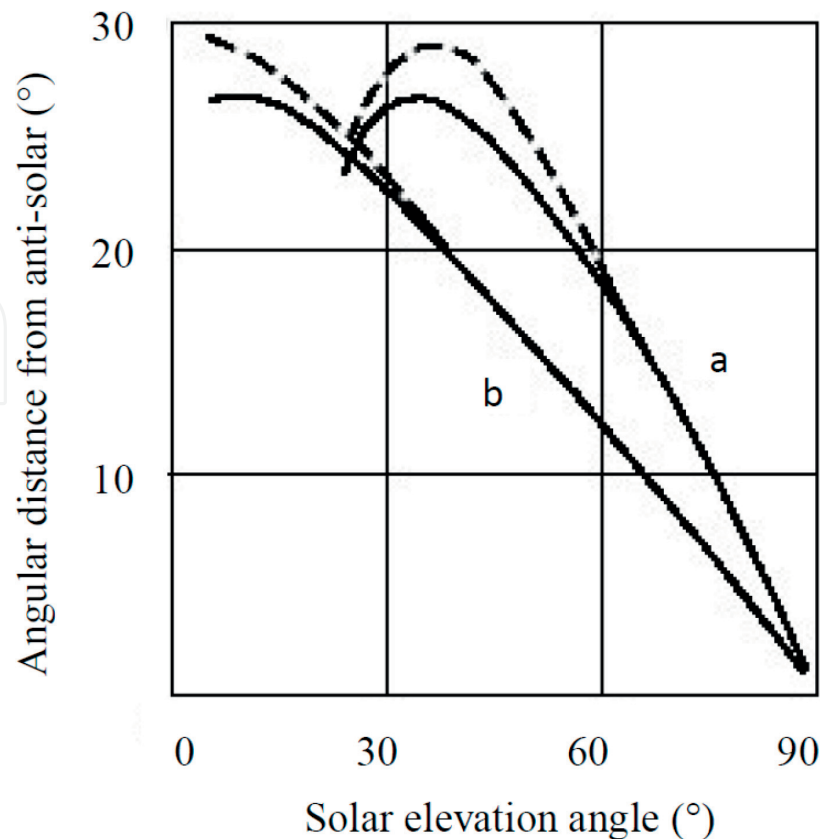


Figure 13. Angular distance between the sun and the neutral points.

25 to 60°. Both the neutral points in the upward (Arago point) and downward (Brewster point) radiation cannot appear in the sky when the solar elevation angle is less than 25°. As for curve (b), the two neutral points' positions in the upward (anti-Babinet point) and downward radiation (Babinet point) are entirely consistent when the solar elevation angle is about 32°–90°. Only when the solar elevation angle is small (about 5°–32°), the positions began to be different slightly.

The above discussion shows that the neutral point positions of the same area observed from space and ground are consistent when the atmosphere optical thickness is small and the solar elevation angle is big. Normally, satellite transit time or aerial remote sensing flight time always choose a high solar elevation, in order to obtain sufficient light conditions. At this time, the space-based neutral point position can be calculated by the ground-based observation position.

Kattawar compared the neutral point positions of different atmosphere optical thicknesses in the upward and downward radiations [29]. The result shows that when the atmosphere optical thickness increased, the Babinet point position changed slightly while the Brewster point changed greatly. The position between anti-Babinet point in the upward radiation and Babinet point in the downward radiation is almost the same when the atmosphere optical thickness is <5. This also indicates that the Babinet point positions of the ground-based and space-based observations are coincident of the same area. This paper also gives the impact of

the surface albedo on the neutral point position. The change of surface albedo has small effect to the neutral point position. But the Brewster point is more sensitive than the Babinet point on the surface albedo impact. The anti-Babinet point in the upward radiation is independent of surface albedo.

3.2.2. *Proper neutral point selected for remote sensing*

There are three common neutral points in the sky. We need to select the most applicable one for the polarization remote sensing. The first satisfied condition is its position in the sky, convenient for remote sensing observation. The second condition is that its position should be more stable.

In the visible-near-infrared remote sensing, satellite transits time or aerial remote sensing flight time always chooses a higher solar elevation, in order to obtain sufficient light conditions. The Arago neutral point can only be observed in the morning or toward evening, and its position in the sky is low when appearing. Its position is always lower than sun. Especially, in high latitude area, the sun cannot reach the zenith position. The Arago point is not suitable for polarized remote sensing. The Brewster neutral point has the same situation. The Brewster point position is bound to be even lower. In addition, the Brewster point is affected by the atmosphere condition and land surface reflection greatly. So, the Brewster neutral point is also not suitable for polarization remote sensing.

In contrast, the anti-Babinet neutral point is an ideal choice for polarization remote sensing. From the earth observing characters of Babinet neutral point, the anti-Babinet point is in the same side of the sun; its position is always higher than the sun. It means that the anti-Babinet point can be observed all the day. Higher elevating angle is a benefit in remote sensing to obtain better light conditions. Moreover, the anti-Babinet point is not sensitive to the atmosphere condition. Its position is more stable in the sky when the atmosphere condition changes.

3.2.3. *The position of neutral point calculated*

The position of the anti-Babinet neutral point can be calculated from the position of the Babinet neutral point, since the two points almost have the same position.

The main factor of the anti-Babinet point position is the solar elevation. So when using anti-Babinet point for land surface polarization observation, the first thing is to determine the observation time.

The solar elevation angle is constantly changing at the same place a day. The sun elevation angle of a place can be calculated by the solar elevation angle formula, as in formula (13).

Generally, good weather conditions are selected for aerial remote sensing flight. For the anti-Babinet neutral point, its position in the main plane is the function of the sun elevation when the optical thickness is 0.10. For convenience, the curve was separated into two parts. Both curves fit as segments.

$$\begin{cases} y = 0.9x + 18 & (0 < x < 30) \\ y = 0.75x + 22.5 & (30 \leq x < 90) \end{cases} \quad (14)$$

where x is the solar elevation angle and y is the Babinet neutral point elevation angle.

For the equatorial region, the solar elevation angle of 90° at noon, the sun illuminates the land surface vertically. All the neutral points are gathered into the sun position. The polarized remote sensing sensor should be in the neutral point region when observing land surface vertically, and this is a special case.

For nonequatorial regions, the sun elevation angle cannot reach 90° at noon. In local noon, the solar elevation angle can be calculated by formula (13). Because both neutral point and sun are at the main plane, the corresponding neutral point position can be calculated from formula (14), and then we can get the remote sensing time. One thing needs to be noted that even the sensor in the sky cannot be exactly at the center of the neutral point, and the region around the neutral point is also a small polarization area; it is also conducive to polarization observation.

3.2.4. Experimental verification

In order to verify the method of using the neutral point for polarization remote sensing, we designed a ground verification experiment. Polarization images were taken and compared from neutral point direction and non-neutral point direction for the same area. **Figure 14** is the observation geometry sketch map. **Figure 14(a)** is the sketch map of neutral point direction observation, while **Figure 14(b)** is the sketch map of non-neutral point direction observation. The degree of polarization of atmosphere is zero on the line through the neutral point and camera. The imaging device was Nikon D200 digital camera with iodine polarizer. 0, 60, and 120° , three angle polarization images, were obtained by changing the angle between polarizer transmission axis and reference axis three times. And then the images of polarization parameters such as degree of polarization and polarization angle were calculated.

Figure 14 is the polarization parameter comparison images between non-neutral point imaging and neutral point imaging. The observation time was 7:20 am and 11:20 am separately, April 29, 2010. At that time, the solar elevation angle was 24.40 and 62.95° separately. According to formula

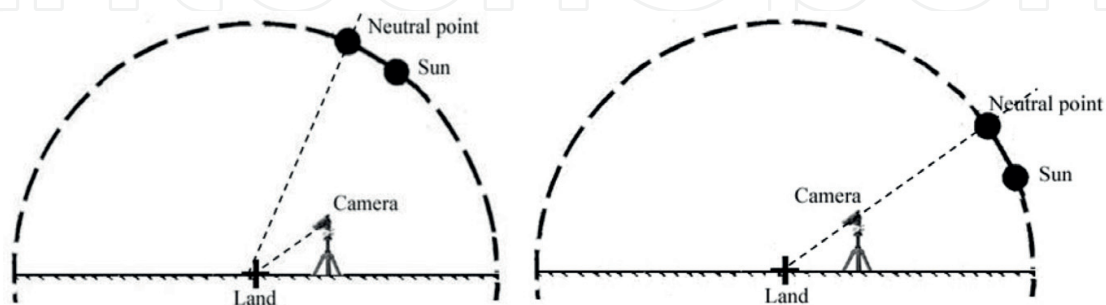


Figure 14. Observation geometry sketch map of ground verification experiment. (a) Observation at non-neutral point direction (in the noon) (b) Observation at neutral point direction (in the morning).

(14), the neutral point elevation angle was 69.71 and 39.96° separately. The solar azimuth was 21.70 and 88.55° (the south is defined as the zero azimuth) separately. Both the camera detection elevation angle was set as 40° . The relative azimuth angle of the camera and the sun were 0° (backward) and 66.85° , respectively. The weather was clear and calm. Observation spots were fifth floor platform, remote sensing building, and Peking University. The target area is Summer Palace scenic region. **Figure 14(a)** is the non-neutral point direction observation. **Figure 14(b)** is the neutral point direction observation.

Figure 15(a) shows the images without polarizer. The atmosphere visibility is high. Both the images are clear: whether observation at the neutral point direction or non-neutral point direction. **Figure 15(b)** shows the linear degree of polarization (*DoLP*) images of R, G, B bands. Degree of polarization is a physical quantity that reflects the polarization size of objects. It is a dimensionless number and the value is 0–1. The white and black areas in the figure denote the big value of *DoLP* and small value of *DoLP* separately. On the image taken from neutral point direction (right image), whether the closer tower of Buddhist Incenses (about 3.1 km from camera) or the Forane Mountain (about 8 km from camera) are clearly visible, especially the bare soil and road in the mountains. And the polarization information is not the same in the red, green, and blue bands. However, on the image taken from non-neutral point direction (left image), the closer objects are better displayed, such as the tower of Buddhist Incense. But the polarization information of the forane objects is much weaker, only the mountain outline can be shown. It means that the polarization information of forane objects cannot be obtained from the non-neutral point direction image. This phenomenon shows that along with the increase of the focusing distance, the atmospheric polarization effects increases, and the polarization information of targets becomes weak.

The information entropies were calculated for the unpolarized images in **Figure 15(a)** and the three bands of *DoLP* images in **Figure 15(b)**, as shown in **Figure 16(a)**. The abscissa is different images and the ordinate is the value of information entropy. The twill denotes entropy value of the non-neutral point imaging and the plaid denotes entropy value of the neutral point imaging. It can be seen from **Figure 16(a)** that the information entropies of the two unpolarized images are almost equal regardless of the neutral point imaging or non-neutral point imaging. However, for the *DoLP* images of red, green and blue bands, the information entropy values of the neutral point imaging are all greater than the non-neutral point imaging. This also shows that land objects on the neutral point *DoLP* imaging are informative. In particular, we cut out the upper half of all the images, keep only the distant objects on the images, and then the information entropies were calculated separately, and the results are showed in **Figure 16(b)**. Similarly, the information entropies of the two nonpolarized images are almost the same. But for the *DoLP* images of red, green, and blue bands, the information entropy values of the neutral point imaging are all much greater than the non-neutral point imaging.

It is thus clear that the atmospheric polarization effect on the non-neutral point direction image is stronger than the neutral point direction image. The degree of polarization image from neutral point direction has good expressive force for remote objects. The objects' polarization information on it is far greater than on non-neutral point direction image's. It means the neutral point imaging can eliminate the atmospheric polarization effect and enhance the objects' polarized information. And then, we had a polarized remote sensing aerial flight experiment with atmospheric neutral

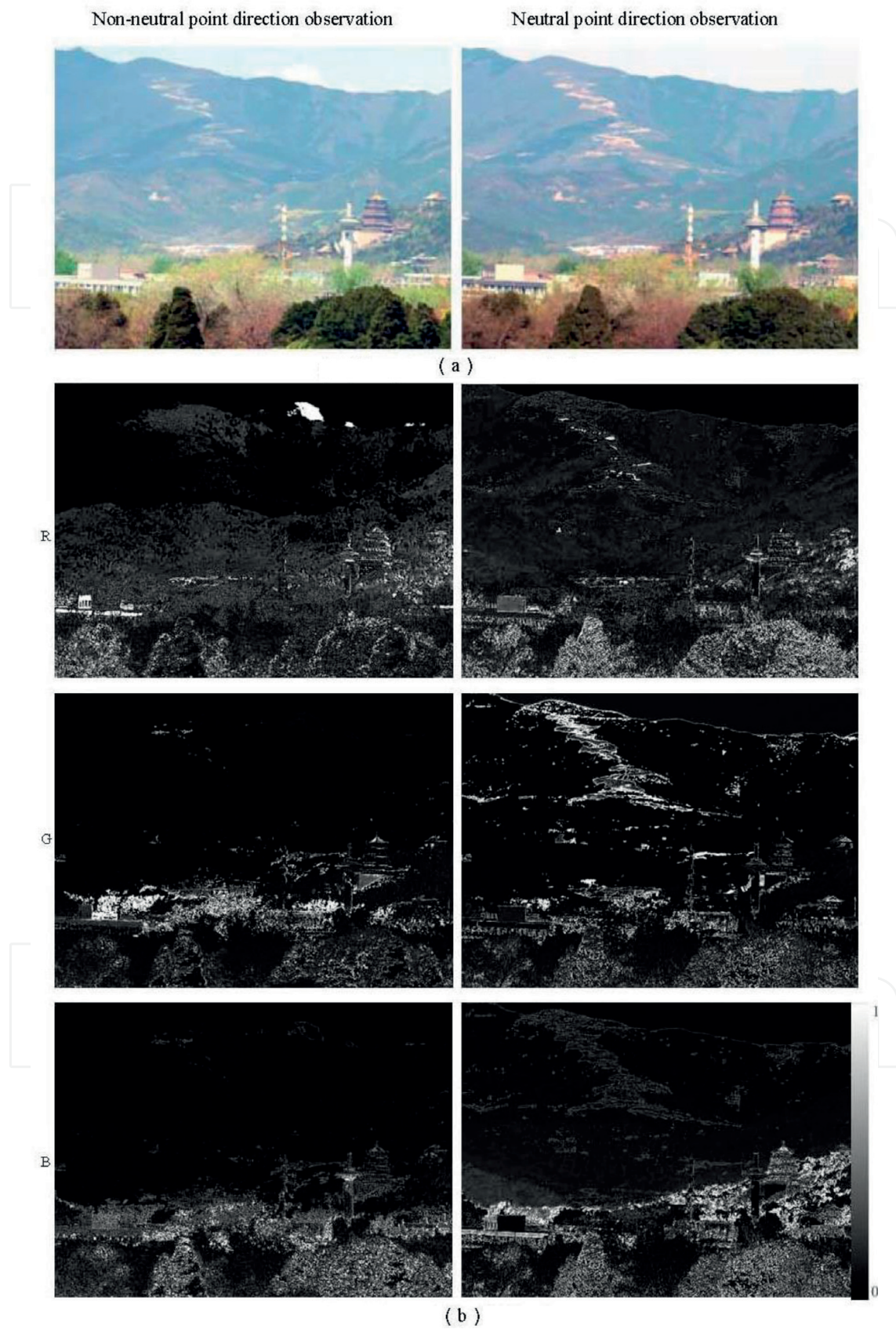


Figure 15. The polarization collation images between neutral point imaging and non-neutral point imaging. (a) Images taken without polarizer and (b) Degree of polarization images.

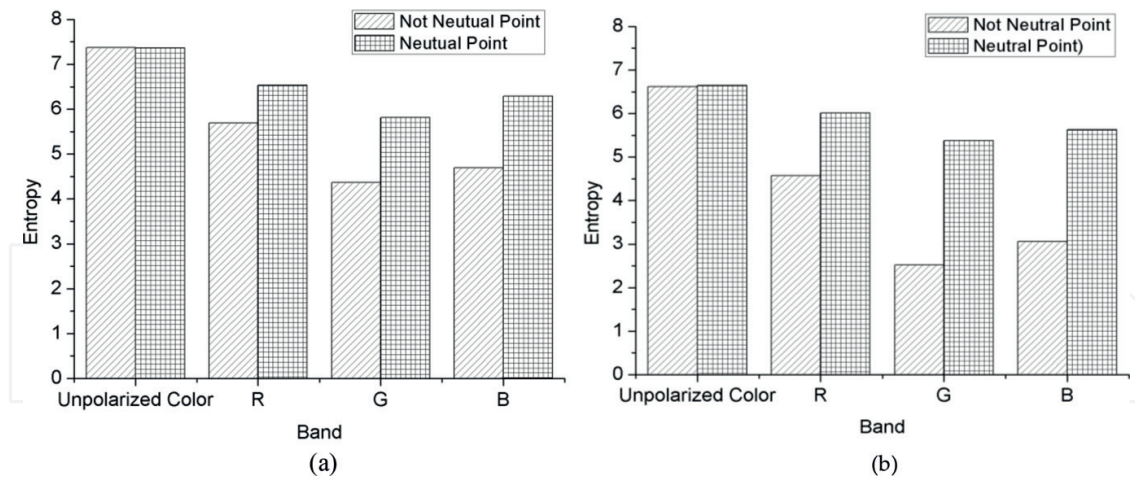


Figure 16. The information entropy comparison between non-neutral point and neutral point imaging.

point [30]. This experiment demonstrated the feasibility of using neutral point for polarized remote sensing in atmospheric correction [31].

4. Conclusion

In conclusion, this chapter showed the researches on land object polarization properties, which can provide a new base knowledge for polarization remote sensing and a new research breakthrough in the separation method for the polarization effect between objects and atmosphere.

1. The polarized bidirectional reflectance characteristics and polarized hyperspectral properties of land objects were methodically studied. It is attempted to find the object polarization reflectance mechanisms by the measurements and theoretical derivations. The results showed that the land object polarization reflectance had the law of bidirectional reflectance and that there was a quantitative relationship between the bidirectional reflectance and the polarized bidirectional reflectance. These two rules can provide the theoretical basis for polarization remote sensing such as the detecting conditions, modeling, and others. This chapter also gave the polarized spectral property of the typical objects. It can be also used as the spectral basis for polarization remote sensing.
2. It proposed a method of using atmospheric neutral point for the separation polarization effect between objects and atmosphere. In this study, we attempted to install the polarization sensor at the direction of the atmosphere point, at the neutral point. In this case, the polarization effect of the atmosphere was reduced to zero and the polarization information of the land surface was maximized. The theoretical derivation and ground experimental results indicated the feasibility of using atmosphere neutral point to separate the polarization effect between object and atmosphere.

Author details

Lei Yan¹, Taixia Wu^{2*} and Xueqi Wang¹

*Address all correspondence to: wutx@hhu.edu.cn

1 School of Earth and Space Sciences, Peking University, Beijing, China

2 School of Earth Sciences and Engineering, Hohai University, Nanjing, China

References

- [1] Horváth G, Gál J, Pomozi I, Wehner R. Polarization portrait of the Arago point: Videopolarimetric imaging of the neutral points of skylight polarization. *Naturwissenschaften*. 1998;**85**(7):333-339. DOI: 10.1007/s001140050510
- [2] Wang Y, Yang C, Li X. Regularizing kernel-based BRDF model inversion method for ill-posed land surface parameter retrieval using smoothness constraint. *Journal of Geophysical Research-Atmospheres*. 2008;**113**(D13):1-11. DOI: 10.1029/2007jd009324
- [3] Taixia W, Yunsheng Z. The bidirectional polarized reflectance model of soil. *IEEE Transactions on Geoscience and Remote Sensing*. 2005;**43**(12):2854-2859. DOI: 10.1109/tgrs.2005.857905
- [4] Herman M, Deuzé JL, Devaux C, Goloub P, Bréon FM, Tanré D. Remote sensing of aerosols over land surfaces including polarization measurements and application to POLDER measurements. *Journal of Geophysical Research-Atmospheres*. 1997;**102**(D14):17039-17049. DOI: 10.1029/96JD02109
- [5] Kochenova S, Lerot C, De Maziere M, Letocart V. Importance of polarization for remote sensing of the Earth's atmosphere. In: EGU General Assembly Conference. 2012
- [6] Deschamps P-Y, Bréon F-M, Leroy M, Podaire A, Bricaud A, Buriez J-C, et al. The POLDER mission: Instrument characteristics and scientific objectives. *IEEE Transactions on Geoscience and Remote Sensing*. 1994;**32**(3):598-615. DOI: 10.1109/36.297978
- [7] Talmage D, Curran P. Remote sensing using partially polarized light. *International Journal of Remote Sensing*. 1986;**7**(1):47-64. DOI: 10.1080/01431168608954660
- [8] Shibayama M, Watanabe Y. Estimating the mean leaf inclination angle of wheat canopies using reflected polarized light. *Plant Production Science*. 2007;**10**(3):329-342. DOI: 10.1626/pp.s.10.329
- [9] Schott JR. *Fundamentals of Polarimetric Remote Sensing*. Vol. 81. Spie Press; 2009

- [10] Yun-sheng Z, Tai-xia W, Bao L, Yang-jie L. Quantitative relationship between multi-angle polarized reflectance and BRDF of rock. *Journal of China University of Mining and Technology*. 2005;**15**(3):192-196
- [11] Cloude S. *Polarisation: Applications in Remote Sensing*. Oxford University Press; 2010
- [12] Zhao Y, Wu T, Hu X, Luo Y. Study on quantitative relation between multi-angle polarized reflectance and bidirectional reflectance. *Journal of Infrared and Millimeter Waves-Chinese Edition*. 2005;**24**(6):441. DOI: 10.3321/j.issn:1001-9014.2005.06.010
- [13] Tonizzo A, Zhou J, Gilerson A, Twardowski MS, Gray DJ, Arnone RA, et al. Polarized light in coastal waters: Hyperspectral and multiangular analysis. *Optics Express*. 2009; **17**(7):5666-5683. DOI: 10.1364/OE.17.005666
- [14] Aron Y. Polarization in the LWIR: A method to improve target acquisition. In: *Proceedings of SPIE 5783, Infrared Technology and Applications XXXI*. Vol. 5783. 2005. pp. 653-661. DOI: 10.1117/12.605316
- [15] Schau HC. Estimation of polarization state from hyperspectral imagery. In: *Proceedings of SPIE 5425, Algorithms and Technologies for Multispectral, Hyperspectral, and Ultraspectral Imagery X*. Vol. 5425. 2004. pp. 470-479. DOI: 10.1117/12.541719
- [16] Wu T, Zhang L, Cen Y, Huang C, Sun X, Zhao H, et al. Polarized spectral measurement and analysis of *Sedum spectabile* Boreau using a field imaging spectrometer system. *IEEE Journal of Selected Topics in Applied Earth Observations and Remote Sensing*. 2013;**6**(2): 724-730. DOI: 10.1109/JSTARS.2013.2255862
- [17] YangJie L, YunSheng Z, XiaoWen L, TaiXia W, LiLi Z. Research and application of multi-angle polarization characteristics of water body mirror reflection. *Science in China. Series D, Earth Sciences*. 2007;**50**(6):946-952. DOI: 10.1007/s11430-007-0009-9
- [18] Yang B, Knyazikhin Y, Lin Y, Yan K, Chen C, Park T, et al. Analyses of impact of needle surface properties on estimation of needle absorption spectrum: Case study with coniferous needle and shoot samples. *Remote Sensing*. 2016;**8**(7):563. DOI: 10.3390/rs8070563
- [19] Fan X, Goloub P, Deuzé JL, Chen H, Zhang W, Tanré D, et al. Evaluation of PARASOL aerosol retrieval over North East Asia. *Remote Sensing of Environment*. 2008;**112**(3):697-707. DOI: 10.1016/j.rse.2007.06.010
- [20] Bicheron P, Leroy M, Hautecoeur O, Bréon FM. Enhanced discrimination of boreal forest covers with directional reflectances from the airborne polarization and directionality of earth reflectances (POLDER) instrument. *Journal of Geophysical Research-Atmospheres*. 1997;**102**(D24):29517-29528. DOI: 10.1029/97JD01330
- [21] Nadal F, Breon FM. Parameterization of surface polarized reflectance derived from POLDER spaceborne measurements. *IEEE Transactions on Geoscience and Remote Sensing*. 1999; **37**(3):1709-1718. DOI: 10.1109/36.763292
- [22] Miyazaki D, Ammar M, Kawakami R, Ikeuchi K. Estimating sunlight polarization using a fish-eye lens. *Information and Media Technologies*. 2010;**5**(1):164-176. DOI: 10.11185/imt.5.164

- [23] Sheng P, Mao J, Li J. Atmospheric Physics. Beijing: Peking University Press; 2003
- [24] Muheim R, Phillips JB, Åkesson S. Polarized light cues underlie compass calibration in migratory songbirds. *Science*. 2006;**313**(5788):837-839. DOI: 10.1126/science.1129709
- [25] Barta A, Bernáth B, Suhai B, Horváth G, Wehner R. First observation of the fourth neutral polarization point in the atmosphere. *Journal of the Optical Society of America. A, Optics, Image Science, and Vision*. 2002;**19**(10):2085-2099. DOI: 10.1364/JOSAA.19.002085
- [26] Horváth G, Varjú D. Polarized Light in Animal Vision: Polarization Patterns in Nature. Springer Verlag; 2004
- [27] Horváth G, Bernáth B, Suhai B, et al. First observation of the fourth neutral polarization point in the atmosphere.[J]. *Journal of the Optical Society of America A Optics Image Science & Vision*. 2002;**19**(10):2085-2099
- [28] Coulson K. Characteristics of the radiation emerging from the top of a rayleigh atmosphere—I: Intensity and polarization. *Planetary and Space Science*. 1959;**1**(4):265-276. DOI: 10.1016/0032-0633(59)90032-7
- [29] Kattawar GW, Plass GN, Hitzfelder SJ. Multiple scattered radiation emerging from Rayleigh and continental haze layers. 1: Radiance, polarization, and neutral points. *Applied Optics*. 1976;**15**(3):632-647. DOI: 10.1364/AO.15.000632
- [30] Yang S, Guan G, Zhao H, Zhao H, Yang B, Zhang W, et al. Airborne validation of ground-object detection from polarized neutral-point atmosphere. *Spectroscopy and Spectral Analysis*. 2013;**33**(9):2525-2531. DOI: 10.3964/j.issn.1000-0593(2013)09-2525-07
- [31] Wu T, Zhang L, Cen Y, Huang C, Zhao H, Sun X. Neutral point consideration for atmospheric correction in polarization remote sensing. *Journal of Remote Sensing*. 2013;**17**:235-247. DOI: 10.11834/jrs.20132156

